Inorganica Chimica Acta 394 (2013) 310–321

Contents lists available at SciVerse ScienceDirect

Inorganica Chimica Acta

journal homepage: www.elsevier.com/locate/ica

Synthesis, characterization, density functional theory calculations, and activity of a thione-containing NNN-bound zinc pincer complex based on a bis-triazole precursor

John R. Miecznikowski [a,*], Jerry P. Jasinski [b], Matthew A. Lynn [c], Swapan S. Jain [d], Elizabeth E. Butrick [a], Anne Elise R. Drozdoski [a], Kerry A. Archer [a], Jason T. Panarra [c]

[a] Department of Chemistry and Biochemistry, Fairfield University, 1073 North Benson Road, Fairfield, CT 06824, USA
[b] Department of Chemistry, Keene State College, 229 Main Street, Keene, NH 03435-2001, USA
[c] Department of Science and Mathematics, National Technical Institute for the Deaf, Rochester Institute of Technology, 52 Lomb Memorial Drive, Rochester, NY 14623, USA
[d] Department of Chemistry, Bard College, P.O. Box 5000, Annandale-on-Hudson, NY 12504-5000, USA

ARTICLE INFO

Article history:
Received 11 February 2012
Received in revised form 2 July 2012
Accepted 3 July 2012
Available online 20 July 2012

Keywords:
NNN pincer ligand
Mononuclear Zn complexes
X-ray crystallography
Cyclic voltammetry
Density functional theory calculations
Aldehyde reductions

ABSTRACT

A novel ambidentate tridentate pincer ligand based on a bis-triazole precursor, was prepared, characterized, and metallated with $ZnCl_2$ to give a new tridentate NNN-bound pincer zinc(II) pincer complex: dichloro(η^3-*N*,*N*,*N*)-[2,6-bis(3-[*N*-butyl]triazol-5-thione-1-yl)]pyridinezinc(II), [(NNN)$ZnCl_2$]. This compound has pseudo-trigonal bipyramidal geometry at the zinc(II) center and exhibits metal–ligand binding that contrasts with our previously reported SNS-bound systems despite the availability of these same donor atoms in the current ligand set. The zinc complex was characterized with single crystal X-ray diffraction, ^{1}H, ^{13}C, and HSQC NMR spectroscopies, and electrospray mass spectrometry. The ligand precursors were characterized with ^{1}H, ^{13}C, and HSQC NMR spectroscopies, and cyclic voltammetry, and were found to be redox active. Density functional calculations, which investigate and support the nature of the NNN binding suggest that the experimentally observed oxidation and reduction waves are not the result of a simple one-electron process. The zinc complex was screened for the reduction of electron-poor aldehydes in the presence of a hydrogen donor, 1-benzyl-1,4-dihydronicotinamide (BNAH), and it was determined that they enhance the reduction of 4-nitrobenzaldehyde. Quantitative stoichiometric conversion was seen for the reduction of pyridine-2-carboxaldehyde.

1. Introduction

Liver alcohol dehydrogenase (LADH) is a zinc metalloenzyme that catalyzes the oxidation of alcohols to aldehydes and ketones as well as the reverse reaction in which ketones and aldehydes are reduced to alcohols [1–3]. The crystal structure of horse LADH has been solved [4]. The catalytically active site contains one zinc(II) metal center, which is pseudo-tetrahedrally ligated with a labile water molecule and a so-called "SNS" ligand environment containing one *N*-histidine and two *S*-cysteine side chains. LADH is an enzyme composed to two polypeptide chains where each polypeptide chain contains active site histidine and cysteine residues that provide the nitrogen and sulfur atoms [5].

Several LADH models have been previously reported. [6–17]. Some zinc model complexes possess SNS donor atoms, but reactivity data was not reported in these studies [9,10,14]. Dołęga reported tri-*tert*-butoxysilatethiolate and imidazole co-ligands that exhibit N_2S_2 or N_3S coordination to Zn(II) ions [7]. Kellogg reported Co(II) complexes that contain a trisubstituted benzene derivative, 3,5-bis(3-mercaptopropoxy)-*N*-[2-(1*H*-imidazol-4-yl)ethyl]benzamide as a model for LADH [12]. In another case, an LADH model complex has been reported for an SSS-bound zinc complex [15], but such a ligand donor environment is different than that found within the enzyme's active site. An N_3S_2 donor set has been reported by Kovacs for zinc complexes [11] and by Koch for cobalt systems [13].

Walton [8] and Vahrenkamp [15] have reported NNN-bound zinc(II) complexes as models for LADH. Walton reported the reaction of an NNN-bound zinc(II) hydroxide complex with methanol to give a zinc(II) methoxide complex. This reaction is related to the displacement of ethanol by water in the zinc active site in liver alcohol dehydrogenase. Vahrenkamp did report reactivity data for the NNN-bound zinc(II) complexes for the reduction of electron-poor aldehydes [15]. Vahrenkamp also published studies of zinc complexes with N_3O_2 donor atoms in which reactivity data for the reduction of electron-poor aldehydes was reported [15].

In an effort to better understand the catalytic activity of LADH, we have previously used a new and unique family of robust SNS

* Corresponding author. Tel.: +1 203 254 4000x2125; fax: +1 203 254 4034.
E-mail address: jmiecznikowski@fairfield.edu (J.R. Miecznikowski).

0020-1693/$ - see front matter © 2012 Elsevier B.V. All rights reserved.
http://dx.doi.org/10.1016/j.ica.2012.07.009

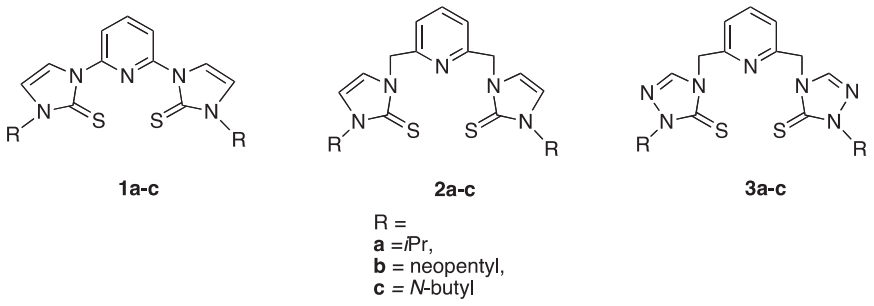

Fig. 1. SNS ligand precursors previously prepared by Miecznikowski et al. [16,17].

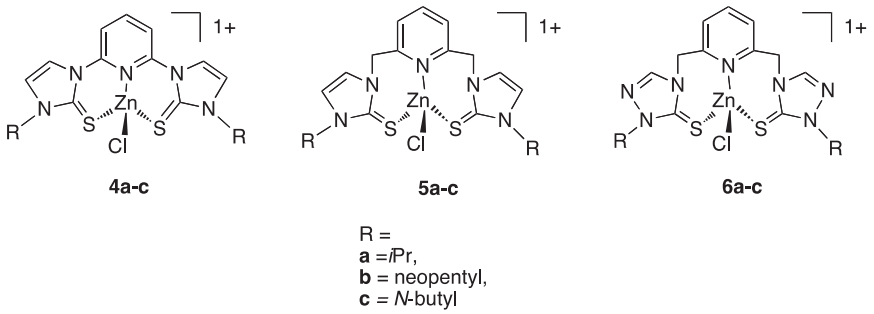

Fig. 2. Zinc-based SNS model complexes previously prepared by Miecznikowski et al. [16,17].

pincer ligands to model the structure and reactivity of the zinc active site in LADH (Fig. 1) [16,17]. Ligands of this type have been used in organometallic chemistry to prepare catalytically active systems, and owing to the tridentate binding mode, compounds that are robust [18,19]. Plus, to the best of our knowledge, such tridentate pincer ligand systems have rarely been used in bio-inspired modeling chemistry, thereby giving us room to explore in this area.

In our past and current studies, we have employed various ligand precursors in an effort to gauge the impact of ligand flexibility on the structure and reactivity of our zinc compounds. We have prepared somewhat rigid ligand systems through the use of 2,6-dibromopyridine as a ligand precursor (Fig. 1, **1a–c**). In these compounds, the imidazolyl groups are directly bound to the pyridine unit such that the flexibility of the ligand is largely limited to rotation about the C—N pyridinyl-imidazolyl bond. In addition, we have prepared more flexible ligand systems by employing the starting material 2,6-(dibromomethyl)pyridine to introduce a methylene linker into the pincer ligand. Use of this precursor has allowed us to compare the effect of ligand flexibility on substrate binding toward the goal of reaching a better understanding of the catalytic activity of LADH whether imidazole(Fig. 1, **1a–c** and **2a–c**) or triazolyl functionalities (Fig. 1, **3a–c**) are used to construct the ligand. The thioimidazolyl *S*-donors have been reported by Parkin and Vahrenkamp to model thiol-derived ligands in bio-inspired zinc chemistry [15,20,21]. Further, our ligands were prepared with imidazolyl or triazolyl rings having wingtip alkyl groups of various sizes (isopropyl, neopentyl, and *n*-butyl) as shown in Fig. 1 in an effort to understand how ancillary alkyl groups affect the ability of the model zinc systems to reduce aldehydes. When 2,6-(dibromomethyl)pyridine was used as a starting material, we were able to fine-tune further the electronic environment imparted by our ligand set by using imidazole- and triazole-based precursors in the preparation of the pincer ligand precursor (Fig. 1, **1a-c**, **2a–c**, and **3a–c**).

Previously, we have prepared zinc model compounds that contain these ligands [16,17] (Fig. 2). In these instances, the pincer ligand exhibits a pseudo-tetrahedral geometry about the zinc(II) center just as is found in the active site of LADH.

After obtaining reactivity results for the reduction of electron-poor aldehydes, we determined that the SNS bis-imidazole Zn complexes that do not contain a CH_2 linker (Fig. 2, **4**) are more active than are those that do contain this connection (Fig. 2, **5**). Conversely, the SNS bis-triazole Zn complexes with a CH_2 (Fig. 2, **6**) linker are more active than are the SNS bis-imidazole Zn complexes without this methylene linker (Fig. 2, **4**) [16,17]. We found that the most active complex for the reduction of 4-nitrobenzaldehyde was an SNS-bound bis-triazole Zn complex with a CH_2 linker and *n*-butyl wingtip groups (Fig. 2, **6c**).

Based on our previous findings regarding the reactivity of the compounds in Fig. 2, we focused our attention in our current work on preparing novel ligand precursors that possess two thione-containing triazole moieties [22] bound directly to the pyridinyl unit. Conceivably, these novel ligand precursors can coordinate to a metal center via either the SNS or NNN donor atoms in the ligand depending on intraligand as well as metal–ligand bonding constraints. Therefore, we present here the synthesis, spectroscopic and electrochemical characterization, computational study, and activity screening of an LADH model system in which our novel tridentate bis(thiotriazolyl)pyridine pincer ligand, in contrast to our previous findings with a similar ligand system, uses only its N atoms to coordinate to a Zn(II) center.

2. Experimental

2.1. General procedures

All reagents used are commercially available and were used as received. All of the reagents and solvents were purchased from Acros Organics except for diethyl ether, sodium acetate, and zinc chloride, which were purchased from Fisher, and pyridine 2-carboxaldehyde which was purchased from Alfa Aesar.

2,6-Bis(1-triazolo)pyridine (btpy) and BNAH were prepared as reported previously [22,23].

NMR spectra were recorded at 25 °C on a Bruker Avance 300 MHz NMR spectrometer. Spectra were referred to the solvent residual peak. Electrospray mass spectrometry was performed on a Varian LC-MS instrument using nitrogen as the drying and nebulizing gas. Cyclic voltammetry experiments were performed using a Cypress Electroanalytical System with a silver wire reference electrode, a glassy carbon working electrode, and a platinum counter electrode. The supporting electrolyte for the cyclic voltammetry experiments was tetra-*N*-butylammonium tetrafluoroborate. The solvent for the cyclic voltammetry experiments was dimethyl sulfoxide. The ferrocenium/ferrocene couple was used as an internal reference; reduction potential values were corrected by assigning the ferrocenium/ferrocene couple to 0.40 V versus SCE. IR spectra were collected using a Thermo Nicolet AVATAR 380-FT-IR with a SMART SPECULATR reflectance adaptor. C, H, N elemental analyses were performed by Atlantic Microlab Inc. (Norcross, GA).

2.2. Crystallographic analyses

A crystal of **9** (*vide infra*) was mounted on a CryoLoop (Hampton Research) and placed in a −100 °C compressed air stream on an Agilent Gemini-EOS Single Crystal Autodiffractometer at Keene State College (Keene, NH). Crystallographic data were collected using graphite monochromated 0.71073 Å Mo Kα radiation and integrated and corrected for absorption using the *CrysAlisRed* (Oxford Diffraction, 2010 software package) [24]. The structures were solved using direct methods and refined using least-square methods on *F*-squared [25]. All other pertinent crystallographic details such as *h*, *k*, *l* ranges, 2θ ranges, and *R*-factors can be found in Table 1.

2.3. Reactivity

In a typical reaction, 0.1 mmol of an electron-poor aldehyde (4-nitrobenzaldehyde or pyridine 2-carboxaldehyde), 0.2 mmol of BNAH, and 0.1 mmol of the zinc complex or 0.1 mmol $ZnCl_2$ were dissolved in 3 mL of $CDCl_3$. The reaction was heated at reflux. Aliquots of the reaction were taken at certain times and analyzed using ^{1}H NMR spectroscopy. All data are averages of at least two runs.

Table 1
Crystal and structure refinement data for $C_{17}H_{23}Cl_2N_7S_2Zn$ [9].

Formula	$C_{17}H_{23}Cl_2N_7S_2Zn$
FW (g/mol)	525.81
Temperature (K)	173(2)
Wavelength (Å)	0.71073
Crystal system	monoclinic
Space group	*P*2(1)/c
a (Å)	11.3556(6)
b (Å)	21.8575(10)
c (Å)	10.3486(4)
β (°)	113.159(5)
Volume (Å)^3	2361.6(2)
Z	4
r (calc) (g/cm^3)	1.461
Absorption (mm^{-1})	1.511
F(000)	1080
Crystal size (mm^3)	0.24 × 0.12 × 0.06
Theta range (°)	3.41–32.33
Reflections/unique	32460/7829
R_{int}	0.0444
Absorption correction	multi-scan
Maximum/minimum	1.0000/0.85028
Reference method	full matrix least squares on F^2
Data/restraints/parameter	7829/0/293
Goodness-of-fit (GOF) on F^2	1.097
R_1 indices ($I > 2s$)	0.0722
wR_2	0.1755
Peak/hole (e/Å^{-3})	2.46 and −0.77

2.4. Gaussian 03 calculations

Gaussian 03 was used to perform single-point calculations and DFT geometry optimizations using the B3LYP hybrid functional with the 6-31G* basis set as provided with the software [26]. Calculations were performed on the unbound and metal-bound ligands with R = Me in all cases. Structures were first optimized in the gas phase as neutral and for the electrochemical analysis, as cationic species under the C_s, C_2, and C_{2v} point groups. Frequency analyses were performed on the optimized structures to determine whether or not they represented true minima. Most structures indicated either no imaginary frequencies or small frequencies on the order of ∼−10 cm^{-1}. The largest imaginary frequencies determined were approximately −40 cm^{-1} and were found for the ligand and metal-bound systems of C_{2v} symmetry. Calculations were also performed in order to obtain an energy profile of the free ligand across the range of pyridinyl–triazolyl dihedral angles possible under the C_2, C_s, and C_{2v} point groups.

Single-point SCRF calculations using DMSO via the CPCM solvent model were performed on the gas-phase optimized structures using the "radii = uff" and "nosymmcav" directives. Oxidation potentials were computed by finding the difference in the total free energies in solution for the neutral and cationic species. These ΔG values were then referenced to the absolute SCE potential in DMSO by subtracting 3.83 V (the established correction to SHE in DMSO) and 0.241 V (the difference between SHE and SCE) [27].

2.5. Syntheses

2.5.1. Preparation of 2,6-bis(3-N-[butyl]triazol-1-yl)pyridine iodide [7]

In a 25 mL round-bottom flask, 0.499 g (1.87 mmol) of 2,6-bis(1-triazolo)pyridine (btpy) was combined with 1.34 g (7.27 mmol) of 1-iodobutane. The neat mixture was stirred at 160 °C for 18 h during which time a white precipitate formed. The solid was taken up in dichloromethane (20 mL) and precipitated with diethyl ether. The solid precipitate was collected via vacuum filtration and was subsequently taken up in methanol and re-precipitated with diethyl ether. The off-white solid was collected via vacuum filtration and was washed with diethyl ether (3x, 30 mL each). Yield: 0.45 g (41%). *Anal.* Calc. for $C_{17}H_{25}I_2N_7$ (581.24): C, 35.13; H, 4.34; N, 16.87. Found: C, 35.60; H, 4.27; N, 17.46%.

^{1}H NMR (DMSO-d_6, 300 MHz) δ 11.39 (s, 2H, triazole, CH), 9.66 (s, 2H, triazole, CH), 8.66 (m, 1H, pyridine CH), 8.31 (d, (^3J = 8.1 Hz), 2H, pyridine CH), 4.46 (m, 4H, *n*-butyl CH_2), 1.97 (m, 4H, *n*-butyl CH_2), 1.41 (m, 4H, *n*-butyl CH_2), 0.96 (m, 6H, *n*-butyl CH_3). ^{13}C {^{1}H} NMR (DMSO-d_6, 75 MHz), δ 145.96 (triazole CH), 145.53 (pyridine CH), 142.02 (triazole CH), 115.21 (pyridine CH), 48.22 (*n*-butyl CH_2), 30.75 (*n*-butyl CH_2), 18.79 (*n*-butyl CH_2), 13.31 (*n*-butyl CH_3).

IR bands (reflectance, powder), ν_{max}/cm^{-1} (intensity): 2954.56 (br), 1611.74 (m), 1565.58 (m), 1501.02 (m), 1457.35 (m), 1446.28 (m), 1405.07 (m), 1367.81 (w), 1207.40 (s), 1065.41 (m). 997.90 (w), 969.67 (s), 911.95 (w), 807.03 (vs), 780.09 (m), 742.13 (w), 721.97 (w), 664.16 (m), 618.10 (vs).

2.5.2. Preparation of 2,6-bis{[N-butyl]triazole-1-ylidene-2-thione}pyridine [8]

In a 250 mL round-bottom flask, 0.501 g (0.862 mmol) of **7** was combined with 0.215 g (2.63 mmol) sodium acetate and 0.747 g (23.3 mmol) sulfur in acetonitrile (35 mL). The solution was heated at reflux for 12 days. After heating, the product was vacuum filtered to remove excess sulfur. The acetonitrile solution was col-

lected and the solvent was removed under reduced pressure. The product was dissolved in dichloromethane and was filtered to remove excess sodium acetate. The dichloromethane solvent was removed under reduced pressure. Yield: 0.33 g (98%). *Anal.* Calc. for $C_{17}H_{23}N_7S_2{\cdot}0.5\ CH_2Cl_2{\cdot}0.5\ H_2O$ (389.54): C, 47.66; H, 5.71; N, 22.17. Found: C, 47.94; H, 5.52; N, 22.96%.

^{1}H NMR (DMSO-d_6, 300 MHz) δ 8.83 (s, 2H, triazole CH), 8.29 (m, 1H, pyridine CH), 8.20 (m, 2H, pyridine CH), 4.01 (m, 4H, *n*-butyl CH_2), 1.75 (m, 4H, *n*-butyl CH_2), 1.32 (m, 4H, *n*-butyl CH_2), 0.92 (m, 6H, *n*-butyl CH_3). ^{13}C{^{1}H} NMR (DMSO-d_6, 75 MHz), δ 166.19(C═S), 148.58 (pyridine C_{ipso}), 142.20 (triazole CH), 140.62 (pyridine CH), 120.46 (pyridine CH), 44.98 (*n*-butyl CH_2), 29.65 (*n*-butyl CH_2), 19.08 (*n*-butyl CH_2), 13.43 (*n*-butyl CH_3).

IR bands (reflectance, powder), ν_{max}/cm^{-1} (intensity): 3427.16 (br), 1651.67 (w), 1622.04 (m), 1598.80 (m), 1559.58 (w), 1451.85 (m), 1406.46 (s), 1334.39 (m), 1297.18 (w), 1236.07 (w), 1204.89 (w), 1158.34 (w), 119.73 (w), 1071.78 (w), 1053.87 (w), 1007.96 (w), 987.58 (w), 966.40 (w), 946.83 (w), 874.89 (w), 812.43 (m), 794.90 (s), 728.91 (w), 669.19 (w).

2.5.3. Preparation of dichloro(η^3-N,N,N)-[2,6-bis(3-[N-butyl]triazol-5-thione-1-yl)]pyridinezinc(II) [$C_{17}H_{23}Cl_2N_7S_2Zn$] [9]

A round-bottom flask was charged with 0.102 g (0.263 mmol) of **8**, 0.0829 g (0.608 mmol) of $ZnCl_2$ and 10 mL of dichloromethane. The solution mixture was refluxed for 24 h. After this time, the dichloromethane was removed under reduced pressure. Single crystals for X-ray diffraction were grown by a slow vapor diffusion of diethyl ether into an acetonitrile solution containing the zinc complex. Yield: 0.11 g (81%). Electrospray MS (MeOH, 20 V, positive ion mode (*m*/*z*): Expected: 488.0 (100%) $[C_{17}H_{23}ClN_7S_2Zn]^+$, Found: 487.9 (100%) $[C_{17}H_{23}ClN_7S_2Zn]^+$. *Anal.* Calc. for $C_{17}H_{23}Cl_2N_7S_2Zn{\cdot}CH_2Cl_2{\cdot}H_2O$ (525.83): C, 34.38; H, 4.33; N, 15.59. Found: C, 33.73; H, 3.79; N, 16.11%.

^{1}H NMR (DMSO-d_6, 300 MHz) δ 8.83 (s, 2H, triazole CH), 8.29 (m, 1H, pyridine CH), 8.20 (m, 2H, pyridine CH), 4.03 (m, 4H, *n*-butyl CH_2), 1.80 (m, 4H, *n*-butyl CH_2), 1.33 (m, 4H, *n*-butyl CH_2), 0.93 (m, 6H, *n*-butyl CH_3). ^{13}C{^{1}H} NMR (DMSO-d_6, 75 MHz), δ 166.24 (C═S), 148.63 (pyridine C_{ipso}), 142.23 (triazole CH), 140.66 (pyridine CH), 120.54 (pyridine CH), 45.03 (*n*-butyl CH_2), 29.70 (*n*-butyl CH_2), 19.12 (*n*-butyl CH_2), 13.48 (*n*-butyl CH_3).

^{1}H NMR (MeOH-d_4, 300 MHz) δ 8.74 (d (^3J = 8.1 Hz), 2H, pyridine CH), 8.29 (t (^3J = 8.1 Hz), 1H, pyridine CH), 4.15 (t (^3J = 7.2 Hz), 4H, *n*-butyl CH_2), 1.87 (m, 4H, *n*-butyl CH_2), 1.45 (m, 4H, *n*-butyl CH_2), 1.01 (m, 6H, *n*-butyl CH_3).

IR bands (reflectance, powder), ν_{max}/cm^{-1} (intensity): 3445.41 (br), 2959.82 (w), 1604.70 (m), 1565.35 (m), 1454.74 (s), 1409.52 (s), 1379.28 (m), 1335.28 (s), 1296.18 (m), 1262.81 (w), 1221.01 (m), 1152.21 (m), 1082.01 (m), 1059.16 (w), 1005.60 (m), 869.97 (w), 814.04 (vs), 736.29 (w), 664.72 (m), 619.30 (m).

3. Results and discussion

3.1. Syntheses and spectroscopy

The synthesis of 2,6-bis{[*N*-butyl]triazole-1-ylidene-2-thione}pyridine, **8**, was accomplished according to the steps shown in Scheme 1. 2,6-Bis(1-triazolo)-pyridine (btpy) was prepared following a published route [22], and was then treated with 1-iodobutane to produce a ligand precursor salt that is more soluble in organic solvents than btpy. Crabtree reported that a wingtip group, *n*-butyl in this case, affects the solubility and catalytic activity of the metal complexes [28]. As such, we find that ligand precursor **7** is soluble in DMSO, methanol, acetonitrile, and water.

Ligand precursor salt **7** was reacted first with a mild base, sodium acetate, and then with elemental sulfur in refluxing acetonitrile to form the bis-thione ligand precursor, **8**, which is soluble in DMSO, dichloromethane, chloroform, acetone, acetonitrile, and methanol. As shown in Scheme 1, isomers of **8** in which the S atoms of the thiotriazole moieties are oriented in a relatively *cis* or *trans* fashion to the pyridinyl N atom are possible. As will be discussed in the computational section, the structure of compound **8** can be idealized and considered under several point groups. It could be planar (C_{2v} symmetry) with both S atoms in either *cis* or

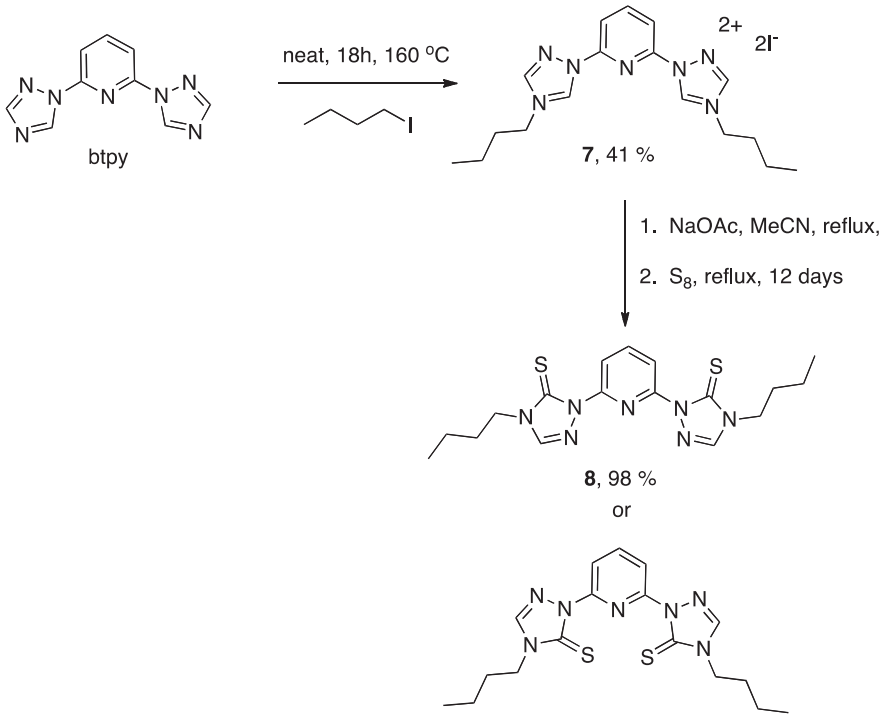

Scheme 1. Preparation of ligand precursors.

trans orientations relative to the pyridinyl N atom. If the system were nonplanar, the highest order point groups under which it can be treated are C_2 and C_s. If one thiotriazole unit is rotated forward and the other backward relative to the pyridinyl unit, the system will have C_2 symmetry. If both thiotriazole units are rotated in the same direction relative to the pyridinyl moiety, the system has C_s symmetry. The calculated energy barrier to thiotriazole ring rotation, to be discussed shortly, is rather low (ca. 9 kcal/mol) so averaging of the NMR signals for the two rings is expected to occur. We are indeed unable to differentiate these various conformations using NMR spectroscopy. We have been unable to obtain a solid-state structure of **8**.

Ligand precursor, **8**, subsequently reacts with excess $ZnCl_2$ in refluxing CH_2Cl_2 to afford zinc complex **9** (Eq. (1)). Excess $ZnCl_2$ was used to drive the reaction to completion. Ligand precursor **8** can conceivably coordinate to the zinc(II) metal center via the SNS donor atoms or via the NNN donor atoms, but we find in the current case that it binds exclusively through only the three available N atoms of the pyridinyl and thiotriazolyl units

Attenuated total reflectance IR spectra were collected for **7**–**9**. All compounds present unique IR spectra. The C=S stretch occurs at 1158 cm^{-1} for the bis-triazole bis-thione precursor, **8**. This data is consistent with the C=S stretching frequencies that we have reported previously for similar compounds [17].

Complex **9** was analyzed with ^1H, ^{13}C, and HSQC NMR spectroscopy in DMSO-d_6. The ^1H and ^{13}C NMR spectra of the zinc complex are similar to those for the ligand precursor, **8**, with little shift in the resonances. Such a result is to be expected since no hydrogen or carbon atoms are displaced or added upon metallation with zinc(II) chloride. Electrospray mass spectrometry data, described below, also verifies this result.

In addition, the ^1H NMR spectrum of complex **9** was also acquired in a less polar and weakly coordinating solvent, MeOH-d_4, to verify that the tridentate pincer ligand is not displaced from the coordination sphere of zinc. In the ^1H NMR spectrum that was acquired in MeOH-d_4, the triazine C—H proton resonance was not observed. We were not able to prepare a sample of **9** in MeOH-d_4 that was concentrated enough to acquire a ^{13}C NMR spectrum.

.

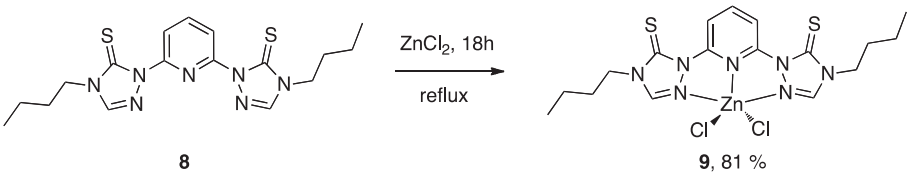

8 **9**, 81 % (1)

The driving force for the metallation is the formation of neutral zinc complex **9**, which is sparingly soluble in CH_2Cl_2. Off-white single crystals suitable for X-ray diffraction were grown by allowing diethyl ether vapor to slowly diffuse into an acetonitrile solution containing the zinc complex. All of the reactions (Scheme 1 and Eq. (1)) were performed in air and proceeded with yields at or above 41%. Zinc complex **9** is soluble in dimethyl sulfoxide, acetonitrile and methanol and is sparingly soluble in dichloromethane and chloroform.

Ligand precursors **7** and **8** and zinc complex **9** were characterized using ^1H, ^{13}C, and HSQC NMR spectroscopy. For all compounds, only one set of resonances was detected. For **7**, the pyridine C_{ipso} was not observed. The ^{13}C NMR of **8** shows a resonance at δ ~166 ppm, that is consistent with C=S formation [16,17,19]. The ligand precursor, **7**, contains a resonance at δ ~11.4 ppm in its ^1H NMR spectrum indicative of a deshielded C—H proton. This feature is absent in the spectrum of compound **8** in which the proton has been replaced by a sulfur atom.

ESI-MS data for complex **9** was collected with a cone voltage of 0 V and 70 V. The predominant feature in the spectrum of **9** is that of the $[(NNN)ZnCl]^+$ ion. This finding suggests that the one chloride ligand is displaced in the mass spectrometer and that the tridentate ligand remains coordinated to the zinc(II) ion. The isotopic pattern in the mass spectrometry data fits the assigned structure.

3.2. X-ray crystallography

The solid-state structure of **9** is shown in Figs. 3 and 4. The complex features a tridentate NNN donor ligand and pseudo-trigonal bipyramidal geometry about the zinc(II) center.

In a five-coordinate geometry, the idealized dihedral angles for the trans basal angle is 158.0°. The distance between Del values for trigonal bipyramid (TP) and square pyramid (SP) structures along the Berry coordinate is 224.7. For complex **9**, using Cl1 as the pivot atom, the TP to SP percentage along the Berry pseudorotation is

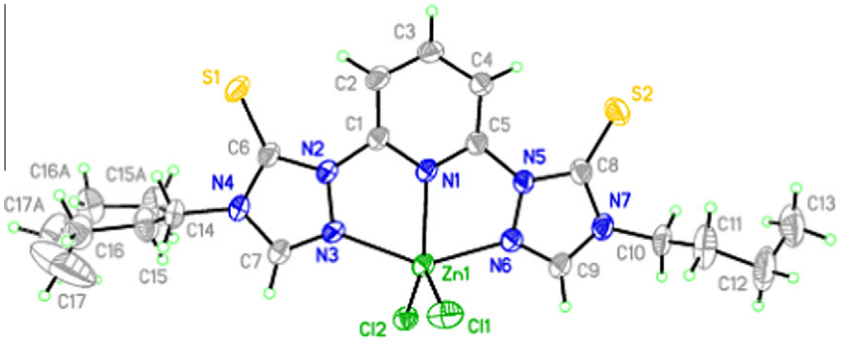

Fig. 3. Molecular structure of **9** showing the atom labeling scheme and 30% probability ellipsoids.

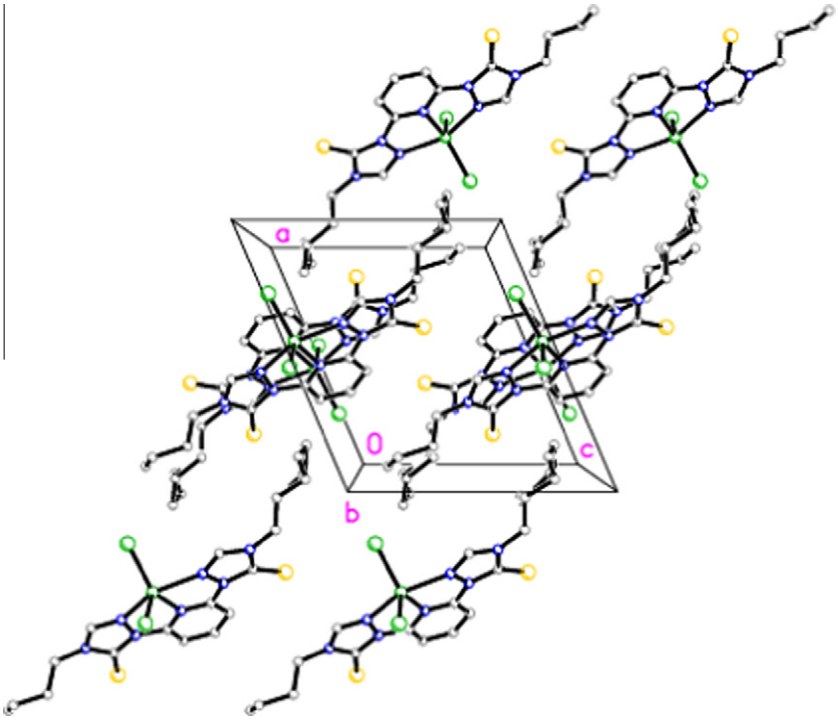

Fig. 4. Packing diagram of **9** viewed along the *b* axis. Hydrogen atoms have been deleted for clarity.

29.5. This value should be zero for a true Berry rotation [29]. The Berry exchange coordinate, based on observed stereochemical nonrigidity associated with five-coordinate species, has been applied to a ground state trigonal bipyramid structure by involving a concerted axial-equatorial bond-bending motion that takes the structure to a square planar transition along a low energy pathway. The motion involves an intramolecular, simultaneous exchange of both axial and equatorial ligands and referred to as the Berry pseudorotation. A plot of the axial angle, θ_{15}, and the equatorial angle, θ_{24}, versus the dihedral angle δ_{24} based on the structural distortion of cyclic phosphorous as one proceeds along a line (referred to as the Berry coordinate), from the idealized square or rectangular pyramid toward a trigonal bipyramid shape provides data for this assignment. The rational is supported by the perturbing influence of packing effects and ligand constraints, if modest, will adjust the penta-coordinated structure along its lowest energy pathway. The dihedral angle, δ_{24} defining the abscissa in the plot is the angle formed between the normal to the trigonal bipyramid faces 124 and 245 that have the common equatorial edge 24 and most intimately associated with the Berry exchange coordinate. This angle has a value of 53.1° for an idealized trigonal bipyramid, but becomes 0° as edge 24 disappears on forming the square (or rectangular) pyramid.

In work related to our own, Turnbull and co-workers have reported the coordination of btpy, our ligand precursor, to a copper(II) ion [22]. They reported an extended coordination polymeric network. The triazole nitrogen atom in btpy coordinates to a copper(II) ion to form an extended coordination polymer. The triazole N atom that coordinates to the copper(II) ion in btpy is coordinated to the *n*-butyl group in complex **9** in our work [22].

Other studies have shown polymeric, ring, and/or zig-zag chain structures when the btpy ligand is coordinated to Rh(II), Ag(I), Fe(III), Zn(II), or Cu(II) ions [30–35]. In all of these complexes, the transition metal ion is coordinated to one of the triazole nitrogen donor atoms and other ligands [22,30–35]. In all of these complexes, the metal atoms bind to the triazole N to which the *n*-butyl groups are bound in our complex **9**. Thus, when btpy is metallated, the NNN donor atoms in the ligand precursor do not coordinate to a single metal atom in a tridentate fashion. Given the difference in metal–ligand coordination that we observe here, we propose that it is the presence of the sterically bulky *n*-butyl wingtip groups in **9** that encourages the ligand to coordinate to a single zinc center in a tridentate fashion.

Various bond lengths and angles for **9** are given in Table 2. The carbon–sulfur bond lengths in **9** are between what is normally associated with a C—S single bond (1.83 Å) and a C═S double bond (1.61 Å) [36]. In **9**, the bond lengths of 1.653 Å and 1.647 Å are closer to that of a C═S double bond than a C—S bond. The Zn—N (pyridine) bond length is consistent with the zinc–nitrogen bond lengths that we and others have previously reported [16,17,37]. The zinc–nitrogen (triazole) bond lengths are about 0.1 Å longer than that of a zinc–nitrogen (triazole) bond length in a previously reported zinc–triazole complex [38]. The zinc–chloride bond

Table 2
Selected bond-lengths and angles (esd) for **9**.

	(**1**)
Zn(1)–N(1) (Å)	2.166(3)
Zn(1)–N(3) (Å)	2.200(3)
Zn(1)–N(6) (Å)	2.165(3)
Zn(1)–Cl(1) (Å)	2.2764(12)
Zn(1)–Cl(2) (Å)	2.3021(10)
C(6)–S(1) (Å)	1.653(4)
C(8)–S(2) (Å)	1.647(4)
N(6)–Zn(1)–N(1)	72.35(12)
N(6)–Zn(1)–N(3)	144.49(13)
N(1)–Zn(1)–N(3)	72.24(12)
N(6)–Zn(1)–Cl(1)	95.98(11)
N(1)–Zn(1)–Cl(1)	119.24(10)
N(3)–Zn(1)–Cl(1)	103.48(11)
N(6)–Zn(1)–Cl(2)	98.56(10)
N(1)–Zn(1)–Cl(2)	122.22(9)
N(3)–Zn(1)–Cl(2)	97.83(10)
Cl(1)–Zn(1)–Cl(2)	118.42(4)

lengths are consistent with those of single bonds in five-coordinate zinc complexes. [39].

The *R*-factor of **1** was 0.07. The higher *R*-factor for **9** was attributed to the disorder in the *n*-butyl groups present in the zinc complex [17,40].

The four five-membered rings present in the structure of **9** (i.e. the two triazolyl units and the two five-membered rings that include the zinc center) are essentially planar with maximum deviations from the mean planes as follows: Zn1/N1/C1/N2/N3 (0.0042(15) Å-Zn1); Zn1/N1/C5/N5/N6 (−0.024(4) Å-N6); N2/N3/C7/N4/C6 (−0.006(4) Å-N4); N5/N6/C9/N7/C8 (−0.005(5) Å-C8). The atoms that comprise the six-membered pyridine ring are coplanar with each other with a maximum deviation from the mean plane of symmetry by 0.005(5) Å-C3, C4.

There is a large residual peak in the final difference map (2.46 e/Å^{-3}) and it is 0.65 Å from Cl1. The large minimum residual peak (−0.77 e/Å^{-3}) is 0.46 Å from Cl2.

3.3. Gaussian 03 modeling of ligand, metal–ligand binding, and cyclic voltammetry results

Recently, we have reported several LADH model complexes constructed of either a bis(imidazolylthione)pyridine or a bis(triazolylthione)pyridine ligand, the latter containing CH_2 linkers within the ligand set, bound to a zinc center [16,17]. In each of these systems, the tridentate ligand was found to bind to the metal center via the pyridinyl N atom and the thionyl S atoms. For the imidazolyl-containing complexes [16], the only atoms available for bonding to the metal center are these three donor atoms whereas two additional N atoms are present in the triazole system [17]. Aside from the N-bound alkyl groups in our previous triazole-based report and our current findings, we note that there are two main structural differences between those compounds and the ones presented herein. First, the N atoms of the triazole employed in our current report are in the 1, 3, and 4 positions relative to the pendant alkyl group whereas in our previous study they were located in the 1, 2, and 4 positions. Second, the organic system in our current report does not possess CH_2 linkers between the pyridinyl and triazolyl moieties whereas the ligand we reported previously does have such a connection. Given the structural differences that we observe through the use of these two similar tridentate ligand systems, we were interested in understanding the geometric and electronic factors that lead to the difference in the preferred metal–ligand bonding configurations in each of these systems. Therefore, we present here an energy analysis of various conformations of the unbound ligand and bound metal–ligand systems to support our current findings followed by an analysis of the oxidation feature we observe in the cyclic voltammogram.

3.3.1. Computational analysis of unbound conformations of 2,6-bis{[*N*-methyl]triazole-1-ylidene-2-thione}pyridine

Given the lack of methylene linkers in our current ligand system, the only way in which the relative orientations of the N and S donor atoms can be modified is by way of rotation about each of the two C—N pyridinyl–triazolyl bonds in the molecule. Through the use of molecular symmetry, we chose to model our ligand set under several point groups in order to understand the overall energetics of the system as well as to deduce intramolecular interactions that give rise to any energy preferences. These point groups are: C_{2v} (the entire molecule, with the exception of several of the H atoms on the pendant methyl groups, is flat), C_2 (the axis of rotation passes through the pyridinyl N atom and the C atom at the 4 position of this ring; one of the triazolyl rings is rotated such that the thionyl S atom is in front of the pyridinyl ring while the other is positioned so that the S atom is behind the pyridinyl ring), and C_s (the plane of symmetry is perpendicular to the plane of the pyridinyl ring and passes through the pyridinyl N and 4-position C atoms; both of the triazolyl rings are rotated so that the S atoms are oriented in the same direction relative to the pyridinyl ring). In performing our computations, we have chosen to define the dihedral angle between the pyridinyl and thiotriazole rings as being 0° when the ligand as a whole is flat and the thionyl S atoms are located in a *cis* orientation to the pyridinyl N atom.

Shown in Fig. 5 is the energy profile obtained by optimizing the structure of the free ligand at fixed pyridinyl–thiotriazolyl dihedral angles from 0° to 180° at 5° intervals under the C_s and C_2 point groups. The energies of all of the optimized structures are presented relative to the structure with lowest energy, the global minimum of the C_2-symmetric structure. As is evident from the plot, the energy profile for the optimizations under each of the point groups possesses two minima and three maxima. The global minimum is located at a dihedral angle of ca. 145° and a local minimum is found at ca. 45°. The global maximum occurs at 0° and local maxima are found near 90° and 180°. Furthermore, across the range of dihedral angles, the C_2-symmetric structures are found to be slightly more stable than are those with C_s symmetry.

Shown in Fig. 6 are several of the optimized structures of 2,6-bis{[*N*-methyl]triazole-1-ylidene-2-thione}pyridine, their relative

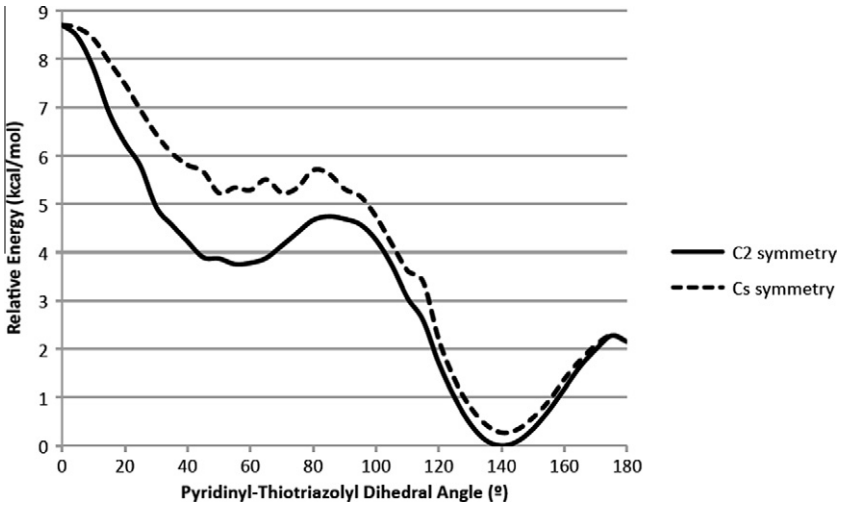

Fig. 5. Relative total energy vs. pyridinyl–thiotriazolyl dihedral angle for 2,6-bis{[*N*-methyl]triazole-1-ylidene-2-thione}pyridine modeled under C_2 and C_s symmetries.

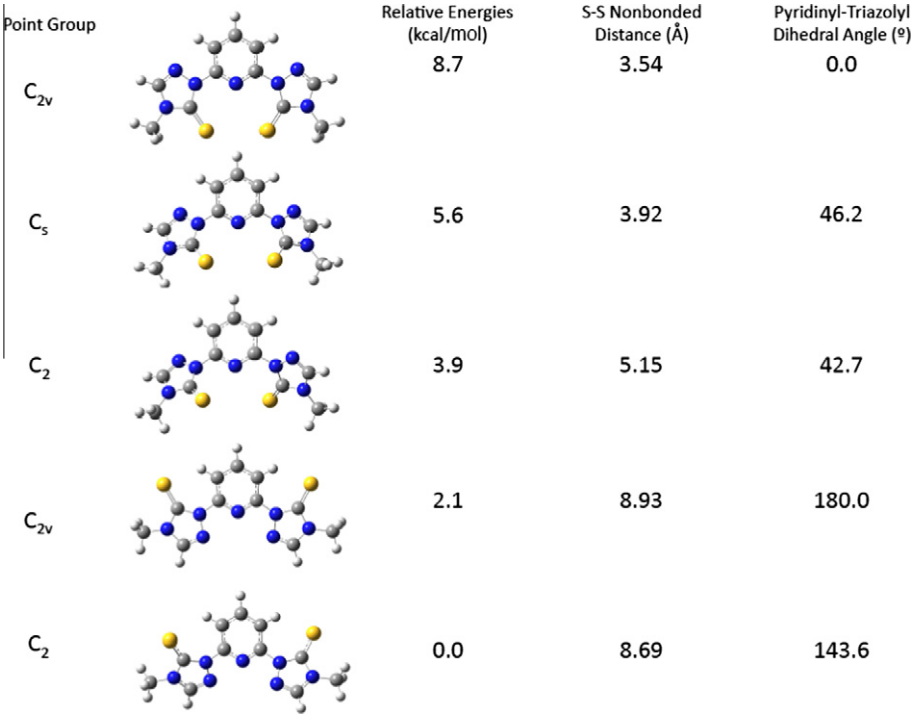

Fig. 6. Various geometry-optimized conformations of 2,6-bis{[*N*-methyl]triazole-1-ylidene-2-thione}pyridine, their relative energies, and structural parameters.

energies, and pertinent structural parameters. In the most stable system (C_2 symmetry), shown at the bottom of this figure, both of the thionyl S atoms are oriented relatively *trans* to the pyridinyl N atom with the triazolyl rings rotated such that they deviate from coplanarity with the pyridine fragment by 143.6°. The analogous C_s-symmetric structure (not shown in the figure) is a mere 0.3 kcal/mol less stable than this C_2 conformation. Confining these *trans* systems to be completely flat with a pyridinyl–thiotriazolyl dihedral angle of 180° destabilizes the molecule by approximately 2.1 kcal/mol relative to the global minimum.

Rotation of the thiotriazolyl rings such that the thionyl S atoms are both relatively *cis* to the pyridinyl N atom destabilizes the molecule relative to the *trans* structures. Local minima are found at dihedral angles of 42.7° (C_2) and 46.2° (C_s); these local minima are 3.9 (C_2) and 5.6 (C_s) kcal/mol less stable than the global minimum. The global maximum occurs when the entire ligand system is flat with a dihedral angle of 0°. This structure is nearly 9 kcal/mol above the global minimum.

We ascribe this relative energy ordering to several features: the electrostatic interaction between the negatively charged electron-donor thionyl S atoms, the establishment or disruption of π-conjugation between the pyridinyl and thiotriazolyl rings, and steric interactions between H atoms on these rings. Our calculations show that the S atoms have Mulliken atomic charges on the order of −0.4. The repulsion between these common negative charges gives rise to an intramolecular repulsion between the thionyl moieties such that the conformations in which the S atoms are far apart, which occurs at large pyridinyl–thiotriazolyl dihedral angles, are the most stable. The trend in intramolecular S—S distances presented in Fig. 6 correlates well with this observation. In the most stable structure, the S atoms are 8.69 Å from each other. Although the S atoms are a bit farther from each other (8.93 Å) in the next most stable structure, the planarity of this system increases the non-bonded interactions between the pyridinyl and thiotriazolyl rings; thus the maximization of π-bonding interactions across these rings is not the deciding factor in determining the most stable structure. In the least stable structure the S atoms are separated by 3.54 Å, the closest S—S distance possible given the imposed constraints. In the other structures with a relatively *cis*-pyridinyl N-thionyl S orientation, the S—S distance is on the order of 4–5 Å.

Our inference from this analysis is that the preferred orientation of the triazolyl rings relative to the pyridinyl ring in the unbound system influences how the ligand as a whole binds to the metal center. With the S atoms oriented in a *trans* manner relative to the pyridinyl N atom, approach of the metal center to this preferred ligand conformation leads to the NNN binding that we observe rather than the SNS binding that we have presented previously. While this finding is certainly an important factor, the actual binding of the ligand to the metal center must also be investigated. We therefore present in the next section an investigation of the metal–ligand system in which the zinc center binds either in an NNN or an SNS fashion under these various symmetries to round out our understanding of the structural energetics of this complex.

3.3.2. Computational analysis of various bound conformations of dichloro(η^3-N,N,N)-[2,6-bis(3-[N-methyl]triazol-5-thione-1-yl)]pyridinezinc(II)

In computing the relative energies of the NNN- and SNS-bound systems, we chose to perform our calculations under the same point groups that were used to investigate the free ligand. Shown in Fig. 7 are the six geometry-optimized structures and their relative energies. On the whole, all of the NNN-bound systems are more stable than the SNS-bound complexes. The most stable structure is the NNN-bound structure that possesses C_{2v} symmetry, with the C_2 and C_s structures being 0.04 and 0.35 kcal/mol less stable, respectively. All of these structures exhibit a pseudo-trigonal bipyramidal coordination environment at the zinc center with the two bound nitrogen atoms of the triazolyl rings occupying positions that are roughly axial. The pyridinyl N atom and the Cl atoms are located in equatorial positions.

Given our previous reports of SNS-bound zinc centers, we were surprised to find that for the current tridentate ligand, the SNS binding mode gives rise to systems that are considerably less sta-

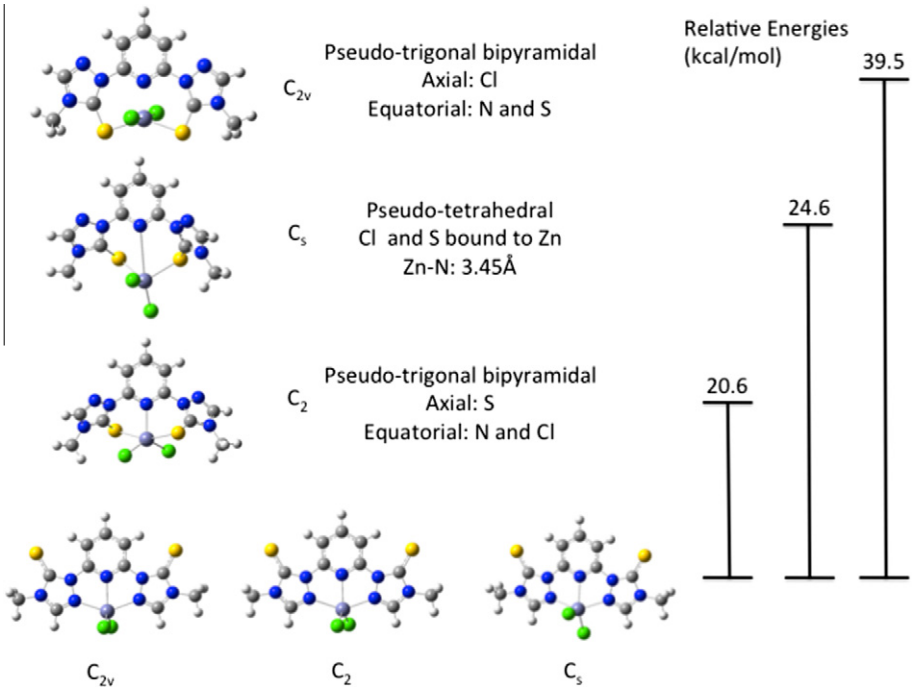

Fig. 7. Various geometry-optimized conformations of dichloro(η^3-*N,N,N*)-[2,6-bis(3-[*N*-methyl]triazol-5-thione-1-yl)]pyridinezinc(II) and their relative energies.

ble. The most stable structure with this binding mode possesses C_2 symmetry and is 20.6 kcal/mol less stable than is the most stable NNN-bound system. The zinc center in this molecule possesses a pseudo-trigonal bipyramidal coordination environment with the sulfur atoms in approximately axial positions. The least stable structure, located nearly 40 kcal/mol above the most stable NNN-bound system, also has a pseudo-trigonal bipyramidal zinc center, but in this structure the Cl atoms are axially bound with the SNS atoms found in equatorial positions. The one structure that we located that does not have this coordination environment is the SNS-bound system that possesses C_s symmetry. In this structure, the Cl and S atoms form a pseudo-tetrahedral environment about the Zn center; the pyridinyl N atom is located 3.45 Å away from the metal center. This structure is reminiscent of an SNS-bound structure that we have previously reported [16]. In that system, two thionyl sulfur atoms, one pyridinyl nitrogen atom, and one chloride formed the coordination environment about the Zn(II) center with a non-ligated counter-anion being present to balance the charge.

The obvious conclusion from these calculations is, given a pseudo-trigonal bipyramidal coordination environment with this ligand system, the NNN-bound system is more stable than one in which the tridentate ligand binds in an SNS fashion. Given that a d^{10} Zn(II) center would not have any ligand field-type preference for a given geometry, we note that the coordination sphere of the metal is predominantly driven by ligand constraints and metal–ligand bonding interactions, including the formation of five-membered rings with the zinc atom and the nitrogen atoms of the pyridinyl and triazolyl fragments. Under the five-coordinate arrangement, the three N atoms are positioned such that they can be arranged in a meridional fashion about the metal center and the π conjugation of the ligand is preserved.

3.3.3. Cyclic voltammetry results and comparison with Gaussian 03-calculated oxidation potentials

Compound **8** was studied by cyclic voltammetry in DMSO as part of its characterization. The cyclic voltammogram for **8** (Fig. 8) shows oxidation features at 706, 1018, and 1311 mV, and reduction waves at −2336 and −786 mV. The oxidation and reduction waves are broad and located at the same potential across consecutive scans. This profile is considerably more complex than what we have observed in previous reports [16,17]. To gain some

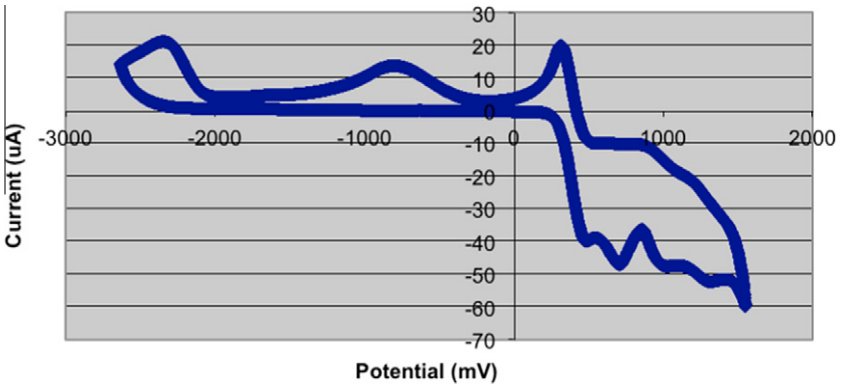

Fig. 8. Cyclic voltammogram of **8** in DMSO (5.6 mM) with 0.2 M TBAF. The scan rate was 100 mV/s with ferrocene ($E_{1/2}$ = 400 mV) used as an internal standard.

insight into this electrochemical feature, we chose to perform quantum mechanical calculations using Gaussian 03.

Unlike in our previous reports, the Gaussian calculations performed as part of this study do not agree well with the experimentally observed oxidation and reduction potentials for the pincer ligand precursor. In those systems, the oxidations were well-behaved and indicative of simple and reversible single oxidations. As such, the oxidation potentials that we calculated using a solvated model and a ΔG method within Gaussian 03 compared well with those that were determined experimentally. We did note in our study of the methylene-linked bis(triazolyl)pyridine system [17] that it was necessary to configure the two triazolyl moieties such that they were stacked to allow the thionyl S atoms to interact *intramolecularly* upon oxidation as has been observed for similar systems that are known to form disulfides upon oxidation [41]. Doing so allowed us to compute an oxidation potential that compared well with what we observed experimentally.

In our current study, however, the triazolyl rings cannot stack due to the lack of a CH_2 linker between the pyridinyl and triazolyl rings. As a result, we computed similar oxidation potentials under each of the three point groups with which we have treated the ligand set: 1743 mV (C_2), 1701 mV (C_s), and 1789 mV (C_{2v}). None of these is particularly close to that observed experimentally (ca. 700–1300 mV). However, given our current computational finding that the most stable conformation of the methyl-substituted version of **8** places the thionyl S atoms *trans* to the pyridinyl N atom and our previous conclusion that oxidation of a similar species results in at least the partial formation of a disulfide bond, we suspect that a simple, reversible, one-electron redox process is not occurring. Rather, electrochemical oxidation of **8** may give rise to the *intermolecular* formation of disulfide bonds, promoted by the *trans* positioning of the thionyl S atoms and resulting in more extended structures that undergo further redox activity as exemplified by the complex cyclic voltammogram reported here.

3.4. Reactivity

Having established a synthetic protocol for this coordination compound and gained an understanding of its structural characteristics, we turned our attention to probing its stoichiometric activity. Compound **9** was screened for activity through the reduction of 4-nitrobenzaldehyde and pyridine-2-carboxaldehyde, both electron-poor aldehydes, in the presence of the hydrogen donor, 1-benzyl-1,4-dihydronicotinamide (BNAH) (Eqs. (2) and (3)). BNAH was prepared following a known literature procedure and is the reagent of choice to model NADH [23].

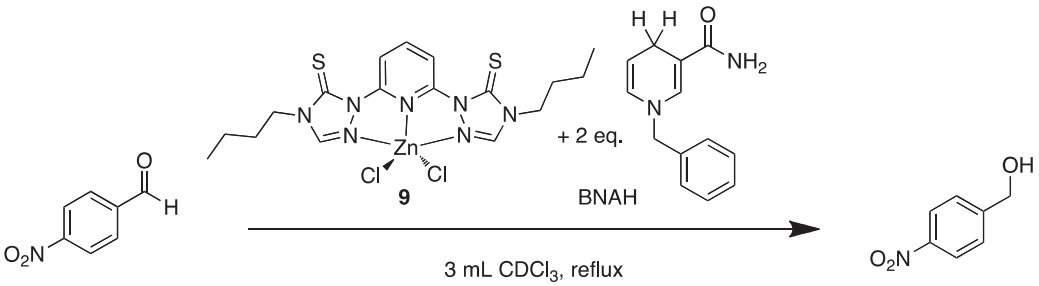

(2)

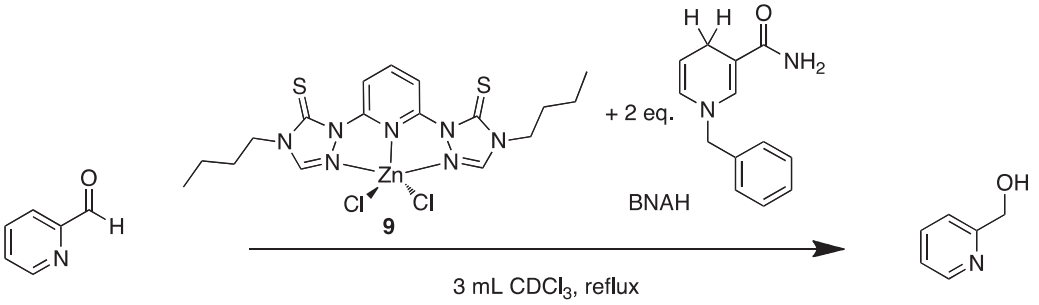

(3)

We have previously reported models for LADH that were screened for activity for the reduction of electron-poor aldehydes using BNAH as a hydrogen atom donor to mimic NADH [16,17]. For the reduction of 4-nitrobenzaldehyde, ^{1}H NMR spectroscopy was used to follow the disappearance of the aldehyde proton (δ 10.2 ppm) and the shifting of the aromatic C—H protons in the alcohol product (δ 8.24 ppm). The resonances of the carbon-bound protons in the alcohol product were spectroscopically distinct from those of the starting materials and no overlap of resonances was observed. For the reduction of pyridine-2-carboxyaldehyde, ^{1}H NMR spectroscopy was used to follow the disappearance of the aldehyde proton (δ 10.2 ppm) and the appearance of the aromatic C—H protons in the alcohol product (δ 8.4 ppm).

Table 3
Stoichiometric reactivity data for the reduction of 4-nitrobenzaldehyde and pyridine-2-carboxaldehyde by ligand precursor **8** or zinc complex **9**.

Entry	Substrate	Zn complex or ligand precursor	Time	Conversion (%)
1	4-Nitrobenzaldehyde	none	20 h	<5
2	Pyridine-2-carboxaldehyde	none	20 h	<5
3	4-Nitrobenzaldehyde	**8**	20 h	<5
4	Pyridine-2-carboxaldehyde	**8**	20 h	<5
5	4-Nitrobenzaldehyde	$ZnCl_2$	20 h	13
6	Pyridine-2-carboxaldehyde	$ZnCl_2$	20 h	13
7	4-Nitrobenzaldehyde	**9**	20 h	35
8	Pyridine-2-carboxaldehyde	**9**	20 h	quantitative

Conditions: 0.1 mmol aldehyde, 0.2 mmol BNAH, 0.1 mmol **9** or 0.1 mmol $ZnCl_2$, and 3 mL $CDCl_3$.

For all reactivity experiments, 0.1 mmol of aldehyde, 0.1 mmol zinc precursor or 0.1 mmol of $ZnCl_2$, and 0.2 mmol BNAH were used. Control reactions with $ZnCl_2$ were performed using one equivalent of this salt because complex **9** contains one zinc ion in the complex. Product formation was detected by ^1H NMR spectroscopy by comparison with authentic material. In no case was there any indication of reduction of nitro substituents. Table 3 illustrates the reactivity data for **9** as well as for $ZnCl_2$ and the ligand precursor.

As shown in Table 3, zinc complex **9** enhances the rate of the reaction for the reduction of 4-nitrobenzaldehyde or pyridine-2-carboxaldehyde when compared to that for either $ZnCl_2$ or ligand precursor. Use of complex **9** results in quantitative conversion of pyridine-2-carboxaldehyde to pyridin-2-ylmethanol. Mechanistically, others have proposed a hydrogen atom transfer between the cofactor and the substrate upon coordination to the zinc active site based upon a previously reported mechanism for LADH offered by Berreau and co-workers [42]. Reactivity data for zinc complex **9** shown in Table 3 for the reduction of 4-nitrobenzaldehyde is lower than SNS bis-triazole zinc(II) complexes we previously reported [16,17].

Entries 5 and 6 in Table 3 indicate that $ZnCl_2$ reacts stoichiometrically with electron-poor aldehydes such as 4-nitrobenzaldehyde or pyridine-2-carboxyaldehyde to yield alcohol product to a small extent (ca. 13% conversion). We therefore propose that Zn^{2+} acts as a Lewis acid catalyst in the reaction where $ZnCl_2$ is utilized.

As seen in Table 3, enhancement for the reduction of 4-nitrobenzaldehyde or pyridine-2-carboxaldehyde was observed for complex **9**. Stoichiometric conversion to the alcohol product was observed for pyridine-2-carboxaldehyde. Pyridine 2-carboxylate may be a good substrate for reduction by **9** since there may be faster hydrogen transfer between the co-factor and the substrate, which is coordinated to the zinc active site. Based on the mechanism proposed by Berreau and co-workers [42], the low activity of complex **9** for the reduction of 4-nitrobenzaldehyde could be due to the slow hydrogen transfer between the co-factor and the substrate, which is coordinated to the zinc active site. More importantly, the alcohol product may inhibit the reaction. As the alcohol is formed, it may coordinate to the zinc metal center as the reaction progresses, and thereby hinder the reaction.

Our work with various benzaldehyde substrates shows that the enzymatic reaction is significantly enhanced in comparison to the model enzyme complexes we have previously reported [16,17]. This work has been done under optimal enzymatic conditions (phosphate buffer, pH 8.8 and 25 °C), which are different than the conditions used in our activity assays with metal complexes. We are currently working with a variety of substrates to probe the effect of electronic and steric factors in our reactions. These results will be presented in a forthcoming paper.

4. Conclusions

A novel Zn(II) complex containing the NNN coordination of a tridentate pincer ligand was prepared and characterized. This zinc pincer complex possesses a pseudo-trigonal bipyramidal geometry about the metal center and reacts with BNAH to reduce electron-poor aldehydes. The zinc complex reacts with BNAH to quantitatively reduce pyridine-2-carboxaldehyde. The zinc complex also reduced 4-nitro-benzaldehyde. Thus, the novel NNN zinc pincer complex reduced aldehydes like LADH.

DFT calculations were performed to examine the electronic properties of the ligand precursor and of the bound zinc system to investigate the nature of the NNN-binding that we have not observed in similar systems. Calculations on the free ligand indicate that the most stable structures possess the thionyl S atoms in a *trans* conformation relative to the pyridinyl N atom. As for the zinc-bound complex, the NNN-ligated arrangement is more stable that the SNS-bound configuration, which we believe is a result not only of the preferred orientation of the free ligand but also of π conjugation across the rings of the ligand. We also find that our computed oxidation potentials do not match well with what is observed experimentally, suggesting that the experimental oxidation does not correspond to a simple one-electron oxidation of the ligand precursor without other reactivity occurring. Our results with complex **9** point to structural features and redox processes that are interesting when compared to our previous reports of SNS coordination of pincer ligands. Furthermore, these results shed new light on the functionality of the LADH active site as studied through the use of model complexes.

Acknowledgements

This work was supported by generous funding from The Fairfield University Science Institute (JRM), Fairfield University Start-up Funding (JRM), Fairfield University Research Grants (JRM), an NTID Faculty Evaluation and Development Grant (MAL), and the Bard Summer Research Institute (SSJ). JRM would like to thank Prof. Matthew A. Kubasik, Prof. L. Kraig Steffen, and Prof. Amanda Harper-Leatherman for helpful suggestions. The authors would like to thank the anonymous peer reviewers that helped improve this article.

Appendix A. Supplementary material

Supplementary data associated with this article can be found, in the online version, at http://dx.doi.org/10.1016/j.ica.2012.07.009.

References

[1] R.H. Holm, P. Kennepohl, E.I. Solomon, Chem. Rev. 96 (1996) 2239.
[2] J.A. Ibers, R.H. Holm, Science 209 (1980) 223.
[3] (a) W.N. Lipscomb, N. Sträter, Chem. Rev. 96 (1996) 2375;
(b) E. Kimura, T. Koike, M. Shionoya, Struct. Bond. 89 (1997) 1.
[4] K.K. Kannan, B. Nostrand, K. Fridborg, S. Lovgren, A. Ohlsson, M. Petef, Proc. Natl. Acad. Sci. USA 72 (1975) 51.
[5] A. Meibner, W. Haehnel, H. Vahrenkamp, Chem. Eur. J. 3 (1997) 261.
[6] A. Dołęga, Coord. Chem. Rev. 254 (2010) 916.
[7] A. Dołęga, A. Pladzyk, K. Baranowska, J. Jezierska, Inorg. Chim. Acta 362 (2009) 5085.

[8] L. Cronin, P.H. Walton, Chem. Commun. (2003) 1572.
[9] L.M. Berreau, M.M. Makowska-Grzyska, A.M. Arif, Inorg. Chem. 40 (2001) 2212.
[10] R.M. Kellogg, R.P. Hof, J. Chem. Soc., Perkin Trans. 1 (1996) 1651.
[11] S.C. Shoner, K.J. Humphreys, D. Barnhart, J.A. Kovacs, Inorg. Chem. 34 (1995) 5933.
[12] (a) B. Kaptein, G. Barf, R.M. Kellogg, F. Van Bolhuis, J. Org. Chem. 55 (1990) 1890;
(b) B. Kaptein, L. Wang-Griffen, G. Bart, R.M. Kellogg, J. Chem. Soc., Chem. Commun. (1987) 1457.
[13] D.T. Corwin, R. Fikar, S.A. Koch, Inorg. Chem. 26 (1987) 3079.
[14] (a) C. Kimblin, T. Hascall, G. Parkin, Inorg. Chem. 36 (1997) 5680;
(b) C. Kimblin, B.M. Bridgewater, D.G. Churchill, G. Parkin, Chem. Commun. (1999) 2301.
[15] (a) R. Walz, H. Vahrenkamp, Inorg. Chim. Acta 314 (2001) 58;
(b) Y.H. Zhang, H. Vahrenkamp, Inorg. Chim. Acta 351 (2003) 201.
[16] J.R. Miecznikowski, W. Lo, M.A. Lynn, B.E. O'Loughlin, A.P. DiMarzio, A.M. Martinez, L. Lampe, K.M. Foley, L.C. Keilich, G.P. Lisi, D.J. Kwiecien, C.M. Pires, W.J. Kelly, N.F. Kloczko, K.N. Morio, Inorg. Chim. Acta 376 (2011) 515.
[17] J.R. Miecznikowski, W. Lo, M.A. Lynn, S. Jain, L.C. Keilich, N.F. Kloczko, B.E. O'Loughlin, A.P. DiMarzio, K.M. Foley, G.P. Lisi, D.J. Kwiecien, E.B. Butrick, E. Powers, R. Al-Abbasee, Inorg. Chim. Acta 387 (2012) 25.
[18] (a) M. Albrecht, G. van Koten, Angew. Chem., Int. Ed. 40 (2001) 3750;
(b) A.T. Normand, K.J. Cavell, Eur. J. Inorg. Chem. (2008) 2781.
[19] D. Morales-Morales, C.M. Jensen (Eds.), The Chemistry of Pincer Compounds, Elsevier, New York, 2007.
[20] (a) C. Kimblin, T. Hascall, G. Parkin, Inorg. Chem. 36 (1997) 5680;
(b) C. Kimblin, B.M. Bridgewater, D.G. Churchill, G. Parkin, Chem. Commun. (1999) 2301;
(c) C. Bergquist, G. Parkin, Inorg. Chem. 38 (1999) 422;
(d) G. Parkin, Chem. Rev. 104 (2004) 699;
B.M. Bridgewater, T. Fillebeen, R.A. Friesner, G. Parkin, J. Chem. Soc., Dalton Trans. (2000) 4494.;
(f) J.G. Melnick, A. Docrat, G. Parkin, Chem. Commun. (2004) 2870;
(g) C. Kimblin, B.M. Bridgewater, D.G. Churchill, T. Hascall, G. Parkin, Inorg. Chem. 39 (2000) 4240.
[21] (a) M. Tessmer, M. Shu, H. Vahrenkamp, Inorg. Chem. 40 (2001) 4022;
(b) J. Seebacher, M. Shu, H. Vahrenkamp, Chem. Commun. (2001) 1026;
(c) Y.H. Zhang, H. Vahrenkamp, Inorg. Chim. Acta 351 (2003) 201;
(d) M.M. Ibrahim, M. Shu, H. Vahrenkamp, Eur. J. Inorg. Chem. (2005) 1388;
(e) R. Walz, H. Vahrenkamp, Inorg. Chim. Acta 314 (2001) 58;
(f) M. Rombach, J. Seebacher, M. Ji, G. Zhang, G. He, M. Ibrahim, B. Benkmil, H. Vahrenkamp, Inorg. Chem. 45 (2006) 4571;
(g) M. Ibrahim, J. Seebacher, G. Steinfeld, H. Vahrenkamp, Inorg. Chem. 44 (2005) 8531.
[22] C.W. Glynn, M.M. Turnbull, Inorg. Chim. Acta 332 (2002) 92.
[23] J. Lutz, F. Hollmann, T.V. Ho, A. Schnyder, R. Fish, A. Schmid, J. Organomet. Chem. 689 (2004) 4783.
[24] Oxford Diffraction, CrysAlis PRO and CrysAlis RED, Oxford Diffraction Ltd., Abingdon, Oxfordshire, England, 2010.
[25] G.M. Sheldrick, Acta Crystallogr. A64 (2008) 112.
[26] M.J. Frisch, G.W. Trucks, H.B. Schlegel, G.E. Scuseria, M.A. Robb, J.R. Cheeseman, J.A. Montgomery Jr., T. Vreven, K.N. Kudin, J.C. Burant, J.M. Millam, S.S. Iyengar, J. Tomasi, V. Barone, B. Mennucci, M. Cossi, G. Scalmani, N. Rega, G.A. Petersson, H. Nakatsuji, M. Hada, M. Ehara, K. Toyota, R. Fukuda, J. Hasegawa, M. Ishida, T. Nakajima, Y. Honda, O. Kitao, H. Nakai, M. Klene, X. Li, J.E. Knox, H.P. Hratchian, J.B. Cross, V. Bakken, C. Adamo, J. Jaramillo, R. Gomperts, R.E. Stratmann, O. Yazyev, A.J. Austin, R. Cammi, C. Pomelli, J.W. Ochterski, P.Y. Ayala, K. Morokuma, G.A. Voth, P. Salvador, J.J. Dannenberg, V.G. Zakrzewski, S. Dapprich, A.D. Daniels, M.C. Strain, O. Farkas, D.K. Malick, A.D. Rabuck, K. Raghavachari, J.B. Foresman, J.V. Ortiz, Q. Cui, A.G. Baboul, S. Clifford, J. Cioslowski, B.B. Stefanov, G. Liu, A. Liashenko, P. Piskorz, I. Komaromi, R.L. Martin, D.J. Fox, T. Keith, M.A. Al-Laham, C.Y. Peng, A. Nanayakkara, M. Challacombe, P.M.W. Gill, B. Johnson, W. Chen, M.W. Wong, C. Gonzalez, J.A. Pople, Gaussian 03, Revision E.01. Gaussian, Inc., Wallingford, CT, 2004.
[27] (a) W.R. Fawcett, Langmuir 24 (2008) 9868;
(b) L.E. Roy, E. Jakubikova, G. Guthrie, E.R. Batista, J. Phys. Chem. A 113 (2009) 6745.
[28] M. Albrecht, J.R. Miecznikowski, A. Samuel, J.W. Faller, R.H. Crabtree, Organomet 21 (17) (2002) 3596.
[29] R.R. Holmes, Progress Inorg. Chem. 32 (1984) 119.
[30] Y. Kim, S.-J. Kim, A.J. Lough, Polyhedron 20 (2001) 3073.
[31] S.-W. Liang, M.-X. Li, M. Shao, H.-J. Liu, Inorg. Chem. Commun. 10 (2007) 1347.
[32] S.J. Hong, J.S. Seo, J.Y. Ryu, J.H. Lee, C. Kim, S.-J. Kim, Y. Kim, A.J. Lough, J. Mol. Struct. 751 (2005) 22.
[33] K.T. Youm, J. Ko, M.-J. Jun, Polyhedron 25 (2006) 2717.
[34] J.Y. Ryu, J.H. Han, J.Y. Lee, S.J. Hong, S.H. Choi, C. Kim, S.-J. Kim, S. Kim, Inorg. Chim. Acta 358 (2005) 3659.
[35] J.Y. Ryu, J.Y. Lee, S.H. Choi, S.J. Hong, C. Kim, Y. Kim, S.-J. Kim, Inorg. Chim. Acta 358 (2005) 3398.
[36] B.V. Trzhtsinskaya, N.D. Abramova, J. Sulfur Chem. 10 (4) (1991) 389.
[37] S.K. Padhi, R. Sahu, V. Manivannan, Polyhedron 27 (2008) 805.
[38] U. Hartmann, H. Vahrenkamp, Inorg. Chim. Acta 239 (1995) 13.
[39] A. Marzotto, D.A. Clemente, G. Valle, Acta Cryst. C50 (1994) 1451.
[40] J.A. Loch, M. Albrecht, E. Peris, J. Mata, J.W. Faller, R.H. Crabtree, Organomet 21 (2002) 700.
[41] A. Suszka, Pol. J. Chem. 54 (1980) 2289.
[42] M.M. Makowska-Grzyska, P.C. Jeppson, R.A. Allred, A.M. Arif, L.M. Berreau, Inorg. Chem. 41 (2002) 4872.